TIME-ACCURATE VERSUS ACTUATOR DISK SIMULATIONS OF PROPELLER SLIPSTREAM FLOWS

XIA Zhenfeng, YANG Yong
Northwestern Polytechnical University, Xi'an 710072, China
xiazhenfeng008@163.com;yyang@nwpu.edu.cn

Keywords: *time-accurate; actuator disk; propeller; slipstream; interference*

Abstract

Two different approaches, time-accurate method and actuator disk theory, are conducted and compared to simulate propeller slipstream flows and its interference with wing. For time accurate simulations, unsteady Reynolds-Averaged Navier-Stokes (RANS) equations are solved by finite volume method based on dynamic-patched grids handling the relative rotation, while quasi-steady state is approaching using actuator disk theory based on point-to-point structured multiblock grids.

A six-bladed propeller is employed, and the unsteady fluctuations of time-accurate velocity distributions in isolated propeller slipstream flows indicate that the blade tip vortices pass by periodically every 60° . The introduction of rotational velocity increase in actuator disk model induces swirls in the flow across the disk making the modeled velocity distributions couples better with the time-averaged ones.

When the propeller installed on the wing, the swirls in slipstream flows alter the wing pressure distributions thus forces. Otherwise, the vorticity distributions in slipstream flows are influenced by wing with staggered locations of blade tip vortices on wing upper and lower surfaces and interacted vortices. The results of actuator disk approach agree well with the time-averaged results of unsteady simulations only with deflection at angle of attack of 10° causing by the induced separation.

1 Introduction

Propeller powered aircrafts are still promising in low speed transports, since they produce larger thrust at low speed with higher economic efficiency and shorter runway requirement, especially because of the high price of fuel[1]. However, the interference between propeller slipstream flows and the aerodynamic components of aircrafts, mainly wing, will influence the aerodynamic capability and stability of the aircrafts[2,3]. Thus, the performance of the propeller and the development of the propeller slipstream flows need to be carefully analyzed.

Computational Fluid Dynamics (CFD) method is greatly helpful for designers to understand and evaluate the complex propeller slipstream flows. There are two main approaches to simulate the propeller slipstream flow and its inference with wing numerically. The first one resolves time-accurate slipstream flows as blades rotate, where grids around the propeller move relatively to the wing based on dynamic patched grid[4] or overlapping grid[5] techniques. Several revolutions are usually required to get the complete evolutionary flow field. The other approach introduces a special boundary condition in the flow at the propeller location to replace the blades, called actuator disk theory[6], which puts the momentum jump and mass flow increase across the propeller on an ideal disk. Since no rotating propeller exists, steady RANS equations are solved, thus much time and computational cost are saved in predictions.

Simulations of an isolated six-bladed propeller and its interference with wing are conducted and compared using both time-accurate method and actuator disk approach. The velocity distributions in isolated propeller

slipstream flows, the influenced wing forces and the interfered slipstream vorticity distributions are presented and analyzed.

2 Computation Strategy

2.1 Time-accurate Method

Three-dimensional time-accurate compressible RANS equations[7] are solved using finite volume method based on body fitted multiblock structured grids. For simulations presented here, spatial discretizations of the convective fluxes are done with second-order upwind Roe's finite-difference splitting scheme, whereas the viscous fluxes are discretized with second-order central difference scheme. Dual time stepping method is employed to advance the solution in time, while multigrid and local time stepping are introduced in the sub iterations to accelerate the convergence. Fully turbulent flow is assumed, and the one-equation turbulent model of Spalart-Allmaras[8] is employed.

To deal with the relative motion between the propeller and the nacelle/wing, dynamic patched grid technique is implemented[9,10]. Patched-grid interpolation coefficients across the cell interfaces are recreated after each physical time step since the relative positions of cells on the two sides of patched faces are renewed.

A six-bladed propeller is adopted here and it is installed on an untwisted wing with symmetric airfoil to simulate the interference. The topology of the dynamic patched grid for isolated propeller, shown in Fig. 1, is comprised of two parts, a cylinder grid surrounding the propeller and the outer grid up to far field boundaries. As the propeller rotates, the inner cylinder grid rotates with the propeller, while the outer part grid keeps stationary with the nacelle. Similar grid topology is employed for the installed configuration, shown in Fig. 2. Although the nacelle in simulations of isolated propeller slipstream flows, shown in Fig. 1, is cylinder to neglect the nacelle geometry effect on slipstream flows, the simulations to identify the install effect are conducted on the same nacelle configuration as that in Fig. 2.

Particular attention should be paid on the grids around the patched surfaces, like shown in Fig. 2. Patching works best when the spacing of the adjacent grid in the normal direction to the patch face is the same as that in the other grid. Too large differences of spacing in the tangential direction will compromise the accuracy of interpolation. To ensure an adequate solution of the blade tip vortices and the wake, very small cells are generated around the blade tip and downstream of the propeller.

For these viscous computations, the total cells amount to nearly 9 million for isolated propeller and 11 million for propeller installed on the wing. And one time-accurate simulation of the installed configuration lasts 5 days on 12 CPU for 5 rotational revolutions to get a fully developed slipstream flows.

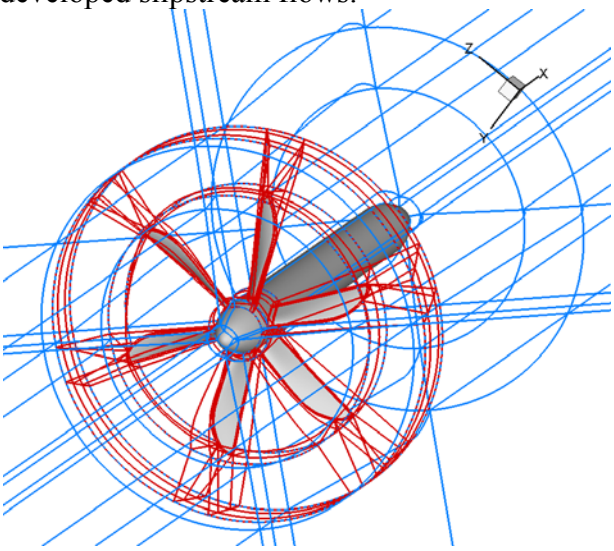

Fig. 1 Grid Topology of Isolated Propeller

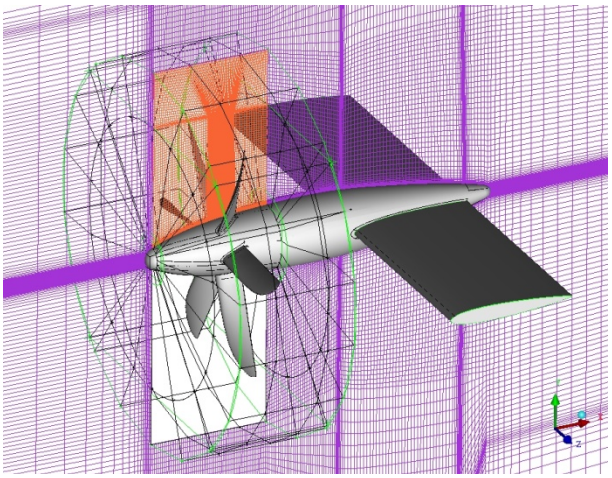

Fig. 2 Grid Topology of Propeller Installed with Wing

2.2 Actuator Disk Approach

According to the momentum theory, the propeller is approximated to be an ideal disk with no thickness, loaded by the momentum variation of flow across the propeller. The load distribution on the actuator disk is the cardinal part for its capability of propeller slipstream flows. To enhance the accuracy, we establish the actuator disk load model from the pressure distributions on the isolated propeller blades[11].

During one rotational cycle of propeller, the axial thrust force T' and tangential force F_θ' on one blade element dr only act during the blade rotates past the angle of $d\theta$, and the time is $dt = d\theta / \omega$. While for the actuator disk approach, the pressure jump Δp and variation of rotational velocity Δv_θ keep on acting on the disk element $dS = rd\theta dr$ during the whole rotation period of $T = 2\pi / \omega$. Since the variation of flow momentum across the area element $dS = rd\theta dr$ needs to be kept the same, the relationships between these variables are given in Eq. (1) and (2),

$$\Delta p \cdot (rd\theta dr) \cdot \frac{2\pi}{\omega} = T'dr \frac{d\theta}{\omega} \cdot N \qquad (1)$$

$$\Delta v_\theta \cdot (\rho u) \cdot (rd\theta dr) \cdot \frac{2\pi}{\omega} = F_\theta' dr \frac{d\theta}{\omega} \cdot N \qquad (2)$$

Where, r is the radius, ω is the rational speed of propeller, N is the number of blades and ρu is product of density and velocity at actuator disk. Axial thrust force T' and tangential force F_θ', which are functions of radius r and azimuth angle θ, are getting from the pressure distributions of isolated rotating propeller blades using time-accurate method.

Quasi-steady RANS simulations are conducted, with the load distributions of pressure jump Δp and variation of rotational velocity Δv_θ as special boundary condition at the actuator disk[12]. The flux discretization scheme and turbulence model are chosen as same as those adopted in time-accurate simulations, and the solver is advanced in time using implicit approximate factorization.

Since no relative motion here, the grid topology adopted is point-to-point structured multiblock. Besides, the grid generation is much easier than the dynamic patched grid due to the simply geometry of ideal disk. The grid, corresponding to the installed propeller configuration, used for actuator disk method is about 4.2 million. Although it is seemingly too fine for this simple geometric configuration, the quasi-steady simulation does not cost too much. One simulation only lasts 6 hours on 4 CPU, which shortens too much CPU time getting a reasonable solution relative to the time-accurate method. The surface grid of installed configuration is shown in Fig. 3, and the grid on actuator disk is also displayed.

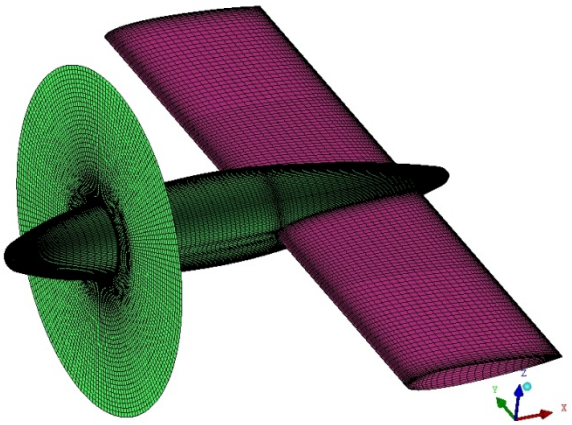

Fig. 3 Grid of Actuator Disk Approach

3 Results and Analysis

Numerical simulations of this six-bladed propeller are performed with fixed rotational speed ω=1075rad/min. With advance ratio λ=0.7, the freestream Mach number *Ma*=0.1475 and Reynolds number *Re*=3.43E06, while at λ=1.1 *Ma*=0.2319 and *Re*=5.4E06 respectively.

3.1 Isolated Propeller Slipstream Flows

The slipstream flow development behind the isolated propeller, at advance ratio λ=1.1 with angle of attack of α=0° is analyzed here.

As the propeller rotates, it induces swirls in the slipstream, and the blade tip vortices in slipstream pass by periodically. Fig. 4(a) (b) show the time-accurate normalized axial and tangential velocity radial distribution in the slipstream just behind the propeller at *x/R* =0.2 respectively, in which *R* is the radius of the propeller and *x*=0 is at propeller location. In Fig.

4, the fluctuations of the time accurate velocity profiles at different rotating blade positions of Ψ=30°, Ψ=60° and Ψ=90° respectively reflect the periodical passage of blade tip vortices, which is significant unsteady performance of the propeller slipstream flow. Since the propeller is six-bladed, the blade tip vortices pass every rotational angle of 60°, which is shown by the superposition of velocity distributions at blade positions of Ψ=30° and Ψ=90°. Furthermore, the amplitudes of fluctuations will decrease downstream in the slipstream.

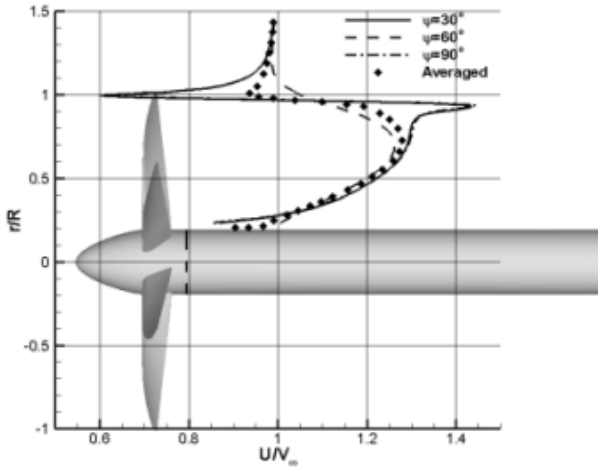

(a) Axial Velocity Profiles

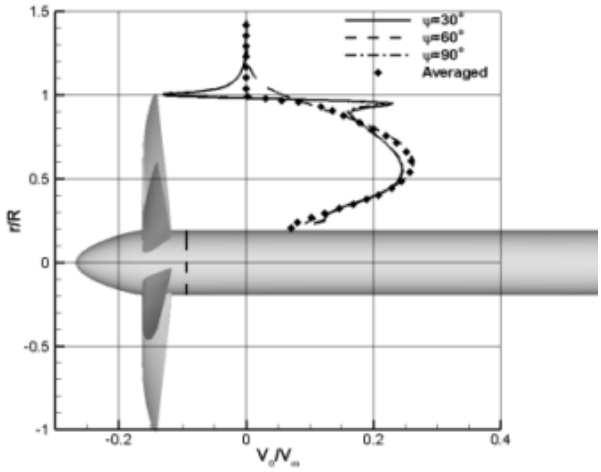

(b) Tangential Velocity Profiles

Fig. 4 Time-accurate radial velocity profiles at x/R=0.2

Since the actuator disk theory approaches the quasi-steady flow, the velocity distributions in slipstream flow will compared with the time-averaged results of unsteady simulations. The comparison of radial velocity profiles downstream the actuator disk at x/R =1.73 is shown in Fig. 5, in which the introduction of rotational velocity increase is also analyzed. In Fig. 5(a), the axial velocity distribution of actuator disk model with both pressure jump and rotational velocity increase couples better with the time-averaged profile of rotating propeller slipstream flow, and Fig 5(b) shows that without introducing rotational velocity increase at actuator disk will not swirl the slipstream flow.

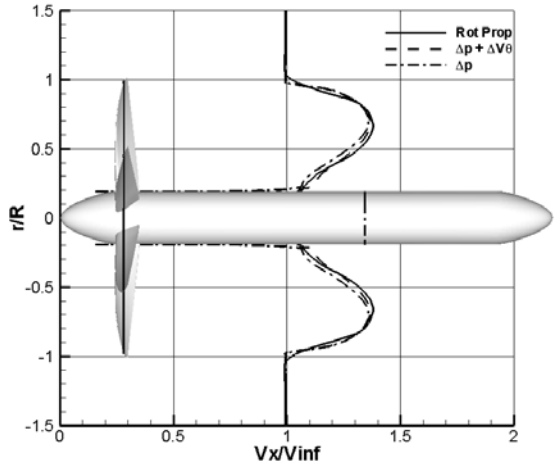

(a) Axial Velocity Profiles

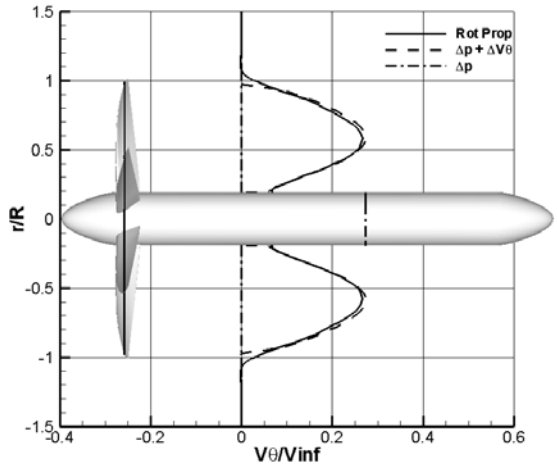

(b) Tangential Velocity Profiles

Fig. 5 Velocity Profiles down Actuator Disk at x/R =1.73

Although we can't get the periodical developments of slipstream flow using actuator disk theory, the well coupled time-averaged velocity distributions and shortened cost are appreciated.

3.2 Installed Propeller

When the propeller is installed on the wing, the slipstream flows influence the wing pressure distributions thus forces, otherwise the presence of wing also interferes with the development of propeller slipstream flows.

3.3.1 Aerodynamic Characteristics of Wing

At angle of attack α=0°, the flow around this wing is symmetric for configuration without propeller. When propeller is installed, the pressure distributions on the wing become antisymmetrical, shown in Fig. 6. That is because the swirls in slipstream flows alter the local angle of attack of sectional airfoils. The swirls sweeping upward increase the local angle of attack, while the other side decreases it. Also shown in Fig. 6, the pressure coefficients of airfoil in slipstream are influenced heavily by the increased velocities in slipstream, especially the pronounced suction peaks at the leading edge. Furthermore, the variation of pressure is larger at lower advance ratio of λ=0.7 than that at λ=1.1.

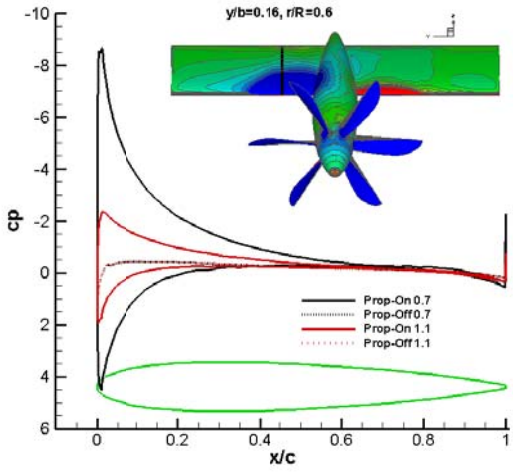

Fig. 6 Influenced Wing Pressure Distributions

As the propeller rotates, the vortices in slipstream flows pass the wing surface periodically. Thus, six sinusoidal oscillations present in the evolution of wing drag during a rotation of the propeller, shown in Fig. 7, due to the six upstream periodically sweeping blades. With propeller installed, the wing drag decreases and the reduction is even larger at λ=0.7 than that of λ=1.1. That is because the suction peak of pressure at the leading edge results to a net pressure force in flight direction.

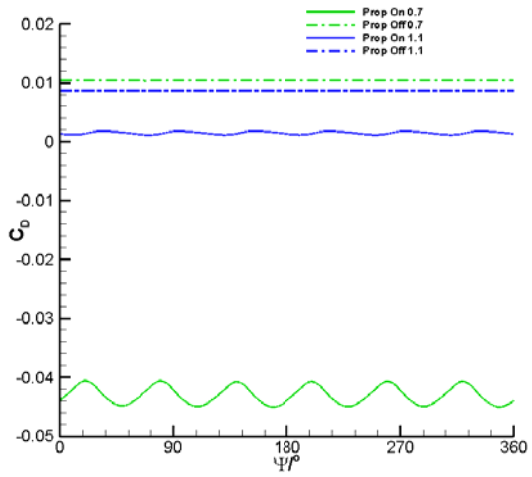

Fig. 7 Wing Drag Evolution during a Propeller Rotation

The characteristics of wing with propeller or not, at different angles of attack with the corresponding advance ratio of λ=0.7, are compared in Fig. 8. Compare with the configuration without propeller, the slipstream always increases the lift and pitching moment magnitudes of wing, while it decreases wing drag at low angle of attack but increase the drag at high angle of attack. The reason that slipstream decrease wing drag at low angle of attack is same as that at angle of attack α=0°. When the angle of attack goes up to 10°, the separation induced may cause the wing drag increasement. The results of actuator disk method couple well with the time-averaged values of unsteady simulations, only with a little deflection at high angle of attack of 10°.

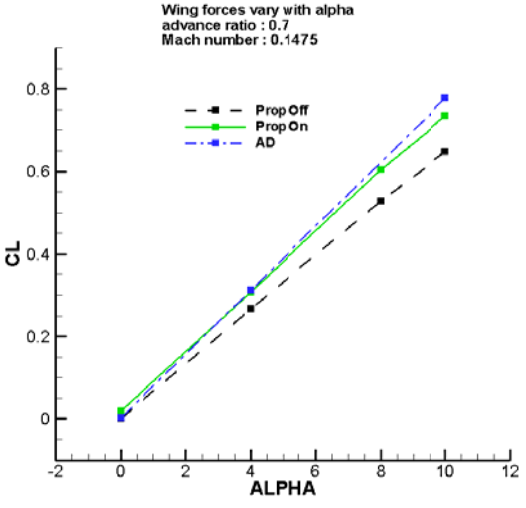

(a) Lift Coefficients

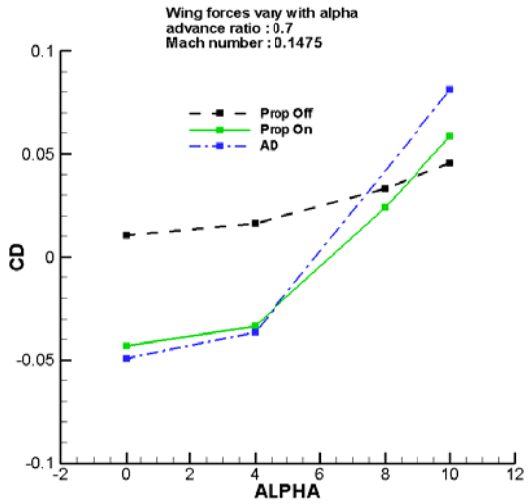

(b) Drag Coefficients

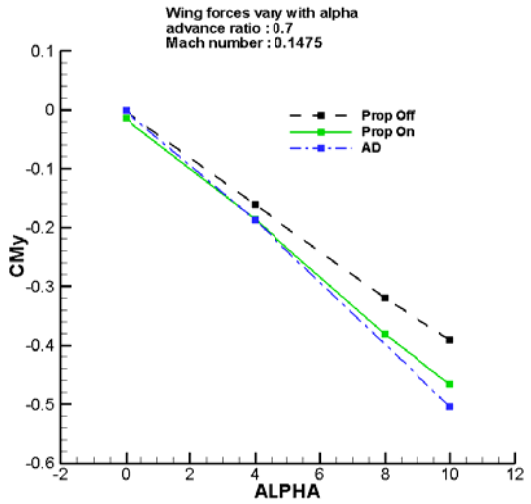

(c) Pitching Moment Coefficients

Fig. 8 Aerodynamics of Wing with/without Propeller

3.3.2 Slipstream Flows

The time-accurate vorticity distributions in the isolated and interacted slipstream flow with advance ratio of λ=0.7 at the angle of attack of α=0° are shown in Fig. 9(a)(b) respectively. The streamwise slices are arranged in X coordinate, between -1.0 and 6.0 with every 0.5 distance a slice, with the wing put nearly between 2.0 and 4.0. The wake flow is heavily affected by the wing. The blade tip vortices shift spanwise outside on one side of the wing and slightly inside on the other side, resulting to be staggered. The streamwise locations of vortices interfered with wing are also staggered between upper surface and lower surface of wing although not shown here.

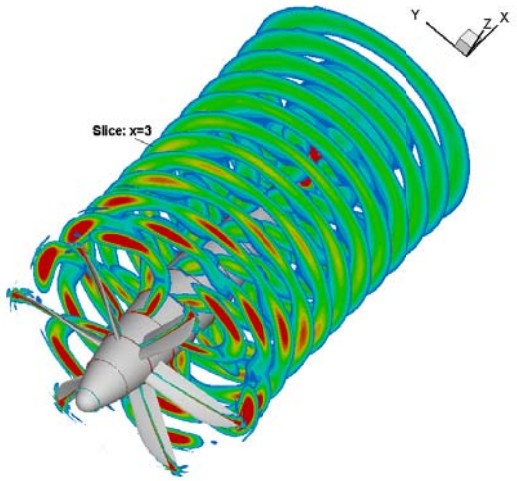

(a) Isolated Propeller Slipstream

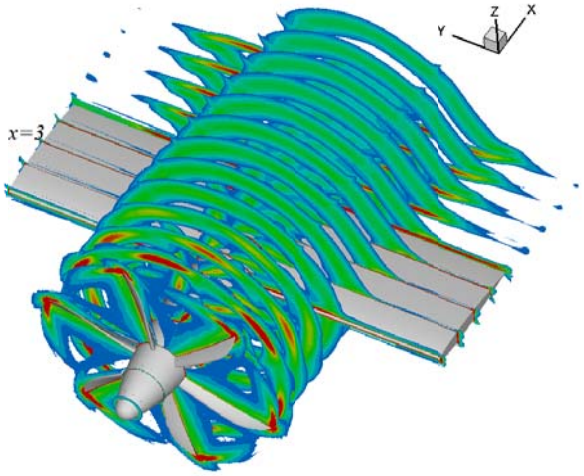

(b) Installed Propeller Slipstream

Fig. 9 Time-Accurate Vorticity Distributions

The vorticity distribution at the location of x=3.0 in Fig. 9 is displayed in Fig. 10(a) to observe the interference more clearly and compared with that of actuator disk approach in Fig. 10(b). Complex interacted vortices present around the juncture of wing and nacelle. Additionally, the original periodical vorticity, shown at slice of x=3.0 in Fig. 9(a), distributes more uniform during the circularity in Fig. 10(a). These important features of interfered slipstream flows are also captured by the actuator disk simulation, shown in Fig. 10(b), although the actuator disk theory only shows the time-averaged state which is determined by its nature.

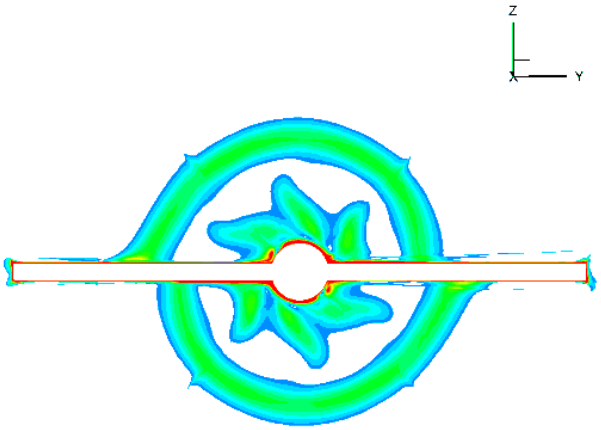

(a) Time-Accurate Method

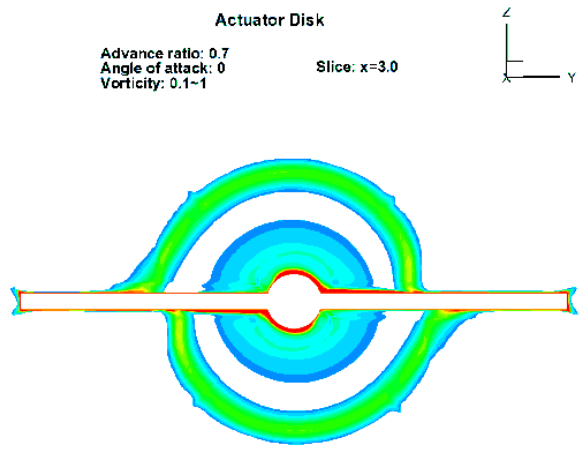

(b) Actuator Disk Approach

Fig. 10 Vorticity Distributions in Slipstream of Installed Configuration at x=3.0 at Angle of Attack of α=0°

When the angle of attack is high, α=10° for example, the upsweeping swirls in slipstream make the local angle of attack for the airfoil even higher. As we all know, separation may happen around the airfoil at high angle of attack. To find out this, the vortices across the streamwise location of x=3.0 of two methods are displayed in Fig. 11(a)(b). The slipstream separates around the sweeping upward side of wing, while no separation happens on the other half part. That is because the swirls upsweeping enlarge the local angle of attack, while they decrease the local angle of attack on the other side. More intricate vortices come forth in Fig. 11 than that at angle of attack of α=0° shown in Fig. 10. The extraordinary complex vortices are due to the interference between the swirls in slipstream and the separated flow. That may cause the deflection of actuator disk method with the time-averaged wing force coefficients of unsteady simulations at angle of attack of 10°.

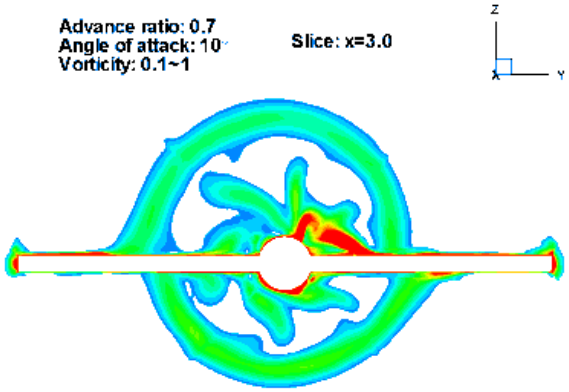

(a) Time-Accurate Vorticity Distributions

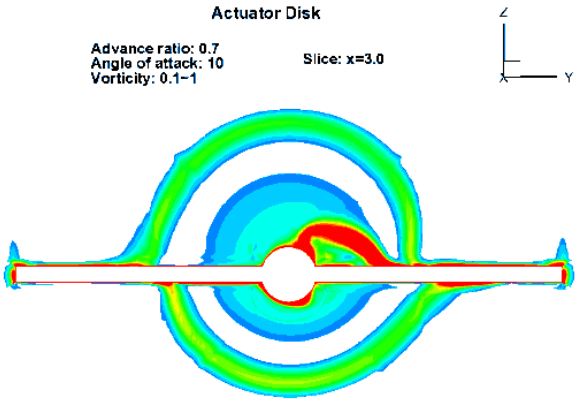

(b) Actuator Disk Approach

Fig. 11 Vorticity Distributions in Slipstream of Installed Configuration at x=3.0 at Angle of Attack of α=10°

4 Conclusions

Time-accurate simulations based on dynamic-patched grids and quasi-steady states approached by actuator disk theory are conducted and compared of isolated propeller and installed propeller on the wing respectively.

For time-accurate simulations, grid generations of the propeller are more complex and much time consuming than that of the simple ideal disk for actuator disk theory.

Moreover, the several revolutions requested in time-accurate simulations cost many times CPU time than the quasi-steady simulations of actuator disk theory.

For isolated propeller, the instantaneous axial and tangential velocity distributions in slipstream flows show the periodical passing by of blade vortices, while those of the actuator disk model introducing the rotational velocity increase couple very well with the time-averaged profiles.

When the propeller installed on the wing, the pressure distributions and forces of wing are influenced by the swirls in slipstream flows. The lift and pitching moment magnitudes of wing are increased while wing drags are decreased at low angles of attack but increased at high angle of attack. Otherwise, the vortices structured in slipstream flows are also interfered by the wing. The streamwise and spanwise locations of blade vortices are staggered on the upper and lower surfaces of wing and interacted vortices are induced near nacelle. Besides, the slipstream flow separates at high angle of attack of 10° around sweeping upward side. The results from actuator disk method agree well with the time-averaged results of unsteady simulations at low and moderate angles of attack however discrepancy appears where separation happens.

The actuator disk approach is particularly attractive in design and prediction period, since it gives a reasonable solution with removing the relative motion which costs too much CPU memory and time in unsteady simulations. However, the time-accurate method is still indispensable when unsteady details are requested as propeller works.

References

[1] Stuermer A. and Rakowitz M. Usteady simulation of a transport aircraft propeller using MEGAFLOW. In *Flow Induced Unsteady Loads and the Impact on Military Applications*. Meeting Proceeding RTO-MP-AVT-123, Paper 7, Neuilly-sur-Seine, France, 2005.

[2] Bousquet J, Gardarein P. Improvements on computations of high speed propeller unsteady aerodynamics. *Aerospace Science and Technology,* No. 7, pp 465-472, 2003.

[3] Roosenboom E., Stuermer A. and Schröder A. Advanced experimental and numerical validation and analysis of propeller slipstream flows. *Journal of Aircraft*, Vol. 47, No. 1, pp 284-291, 2010.

[4] Bohbot J, Grondin G, Corjon A, Darracq D. A parallel multigrid conservative patched/sliding mesh algorithm for turbulent flow computation of 3D complex aircraft configurations. AIAA-2001-1006, 2001.

[5] Stuermer A. Unsteady Euler and Navier-Stokes simulations of propellers with the unstrucutred DLR TAU-code. In: Rath J, Holze C, etc. *New Results in Numerical and Experimental Fluid Mechanics V*. Springer, 2006, pp 144-151.

[6] Veldhuis L. *Propeller wing aerodynamic interference*. Phd thesis, Delft University of Technology, 2005.

[7] Rumsey C, Sanetrik M, Biedron R, etc. Efficiency and accuracy of time-accurate turbulent Navier-Stokes computations. *Computers & Fluids*, Vol. 25, No. 2, pp 217-236, 1996.

[8] Spalart P, Allmaras S. A one-equation turbulence model for aerodynamic flows. AIAA-92-0439, 1992.

[9] Xia Z F, Yang Y, Jiao J. Unsteady simulations of propeller flows based on dynamic patched-grid. *Proceedings of 2010 Asia-Pacific International Symposium on Aerospace Technology,* Xi'an China, Vol. 1, pp 420-423, 2010.

[10] Xia Z F, Yang Y. Unsteady numerical simulation of interaction effects of propeller and wing. *Acta Aeronautica et Astronautica Sinica*, Vol. 32, No. 7, pp 1195-1201, 2011.

[11] Xia Z F, Luo S, Yang Y. Numerical simulations of propeller slipstream flows using actuator disk theory. *Acta Aerodynamica Sinica*, Vol. 30, No. 2, pp 220-224, 2012 (*in press*).

[12] Zuo S H, Yang Y. Numerical simulation of propeller/high-lift system interaction. *Aeronautical Computing Technique*, Vol. 37, No. 1, pp, 54-57, 2007.

Copyright Statement